

www.acsami.org Research Article

Regulation of Osteogenic Differentiation of hBMSCs by the Overlay Angles of Bone Lamellae-like Matrices

Shuyun Zhang, Dengjian Qu, Bowen Luo, Lichen Wang, Hong Li, and Hongjun Wang*



Cite This: ACS Appl. Mater. Interfaces 2024, 16, 56801-56814



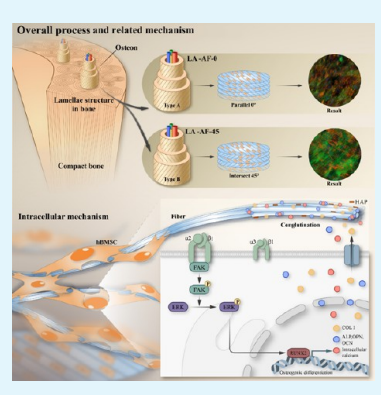
ACCESS I

III Metrics & More

Article Recommendations

s) Supporting Information

ABSTRACT: Oriented fibers in bone lamellae are recognized for their contribution to the anisotropic mechanical performance of the cortical bone. While increasing evidence highlights that such oriented fibers also exhibit osteogenic induction to preosteoblasts, little is known about the effect of the overlay angle between lamellae on the osteogenic differentiation of bone marrow-derived mesenchymal stem cells (BMSCs). In this study, bone lamellae-like fibrous matrices composed of aligned core—shell [core: polycaprolactone (PCL)/type I collagen (Col I) + shell: Col I] nanofibers were seeded with human BMSCs (hBMSCs) and then laid over on each other layer-by-layer (L-b-L) at selected angles (0 or 45°) to form three-dimensional (3D) constructs. Upon culture for 7 and 14 days, osteogenic differentiation of hBMSCs and mineralization within the lamellae assembly (LA) were characterized by real-time PCR, Western blot, immunofluorescent staining for osteogenic markers, and alizarin red staining for calcium deposition. Compared to those of random nanofibers (LA-RF) or aligned fibers with the overlay angle of 45° (LA-AF-45), the LA of aligned fibers at a 0° overlay angle



(LA-AF-0) exhibited a noticeably higher osteogenic differentiation of hBMSCs, i.e., elevated gene expression of OPN, OCN, and RUNX2 and protein levels of ALP and RUNX2, while promoting mineral deposition as indicated by alizarin red staining and mechanical testing. Further analyses of hBMSCs within LA-AF-0 revealed an increase in both total and phosphorylated integrin β 1, which subsequently increased total focal adhesion kinase (FAK), phosphorylated FAK (p-FAK), and phosphorylated extracellular signal kinase ERK1/2 (p-ERK1/2). Inhibition of integrin β 1 and ERK1/2 activity effectively reduced the LA-AF-0-induced upregulation of p-FAK and osteogenic markers (OPN, OCN, and RUNX2), confirming the involvement of integrin β 1-FAK-ERK1/2 signaling. Altogether, the overlay angle of aligned core—shell nanofiber membranes regulates the osteogenic differentiation of hBMSCs via integrin β 1-FAK-ERK1/2 signaling, unveiling the effects of anisotropic fibers on bone tissue formation.

KEYWORDS: core—shell nanofiber, hBMSC, osteogenic differentiation, layer-by-layer stacking, integrin β 1

1. INTRODUCTION

Clinically, healing of large bone fractures such as segmental bone defects (due to a traffic accident or illness) remains a big challenge, which oftentimes leads to nonunion repair even after a prolonged period. In recognition, extensive efforts have been made to develop various osteogenic bone grafts such as the decellularized allogenic bone matrix, bioglass, and CaPcontaining composite with an intention to provide the necessary support for new bone development. While demonstrating their potentials favoring bone regeneration, such acellular grafts are not able to bridge the large defect due to the limited infiltration of bone-forming cells. As such, incorporation of bone-forming cells into such acellular bone grafts for reconstructive surgery becomes a highly viable strategy for timely regeneration of osseous tissues within large defects. Among several bone-forming cells, bone marrowderived mesenchymal stem cells (BMSCs) have received great attention, considering their high osteogenic differentiation capacity. To facilitate regeneration, it would be desirable to explore all possible stimulatory mechanisms in order to identify those determinant factors to maximize the osteogenic differentiation of BMSCs. Cumulative evidence has shown that osteogenic differentiation of human BMSCs (hBMSCs) is orchestrated by various physicochemical factors like mechanical stimulation, inorganic composition, and osteogenic factors and closely regulated by their residing microenvironment such as the substrate stiffness and patterned substrate surface, which typically involve the membranous receptors to relay the environmental cues for further intracellular regulation.

As noted, the osseous tissue in our body is anisotropic and organized in a highly ordered hierarchy to accommodate the need of unique mechanical loads.⁶ Such an anisotropy is realized through the mineralized extracellular matrix, which is composed of organic collagen fibrils encased by platelike

Received: July 31, 2024 Revised: September 17, 2024 Accepted: September 26, 2024

Published: October 10, 2024





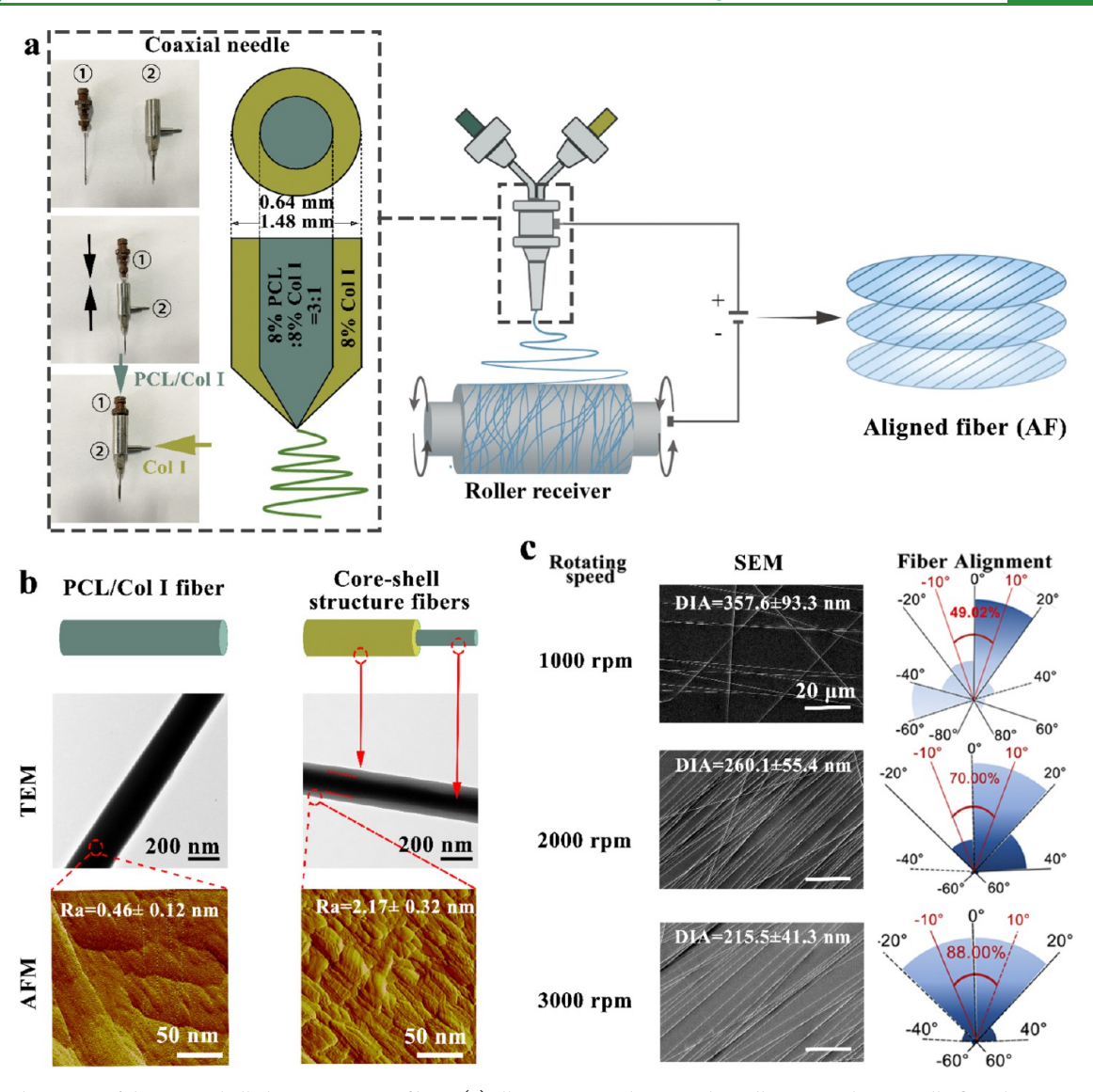


Figure 1. Fabrication of the core—shell electrospun nanofibers. (a) Illustration on the coaxial needle setup, where needle 1 is the inner core needle nested inside needle 2 for the shell. (b) Representative transmission electron microscopy (TEM) and atomic force microscopy (AFM) micrographs of as-prepared nanofibers with or without the core—shell structure to confirm the presence of the core—shell structure and show the surface topographical features. (c) Representative scanning electron microscopy (SEM) micrographs of electrospun fibers collected on the rotating mandrel at different speeds. The diameters (DIA) and Nightingale rose diagram of nanofiber orientations were obtained based on randomly selected SEM micrographs (n = 5).

inorganic hydroxyapatite (Hap) crystals with their c-axes parallel to the longitudinal axis of collagen fibrils. To endure the mechanical load, collagen/Hap fibrils are oriented with a unique spatial organization, and this is particularly true for the load-bearing cortical bone, a packed array of repeating building units of osteons. Each osteon comprises concentric lamellae of collagen/Hap fibers, which are parallel within the lamellae but angled between lamellae. Notably, different overlay angles (0, 30, 45, or 60°) are seen in the mammalian skeleton.^{7,8} In contrast to the comprehensive study on the correlation of superimposed collagen/Hap fibers with the tissue mechanical performance, limited efforts have been made to understand how the overlay angle of lamellae affects the cells sandwiched in between the lamellae, partially due to the lack of an effective model system. To this end, it is highly desirable to establish a platform allowing the generation of the lamellae-like structures with a control of fiber organization and form the overlay assembly at arbitrary angles. With such a platform, the effects

of the angular configuration of the lamellae assembly on osteogenic differentiation of hBMSCs can be better revealed. Thereby, we hypothesize that electrospun fibrous matrices can emulate the lamellae while allowing to recapitulate the angular lamellae assembly via layer-by-layer (L-b-L) stacking of cellladen fibrous matrices (lamellae-like layer). By modulating the electrospinning conditions and fiber collection, fibrous matrices composed of parallel oriented fibers can be obtained to emulate the lamellae structure. We have found that parallel fibers induce the elongation of preosteoblasts (MC 3T3-E1) and promote their osteogenic differentiation, leading to noticeable mineralization. 10 Taking advantage of the high flexibility to vary the superimposing angles during L-b-L stacking, the lamellae assembly with a similar structural organization to the native one can be readily achieved. However, it remains unclear how the superimposing angles during the lamellae assembly affect the osteogenic differentiation.

In this study, core—shell nanofibers were fabricated by using coaxial electrostatic spinning technology. The core made of the polyblend of polycaprolactone (PCL) and type I collagen (Col I) could provide mechanical strength and structural stability, while the shell contained only Col I to endow periodic architecture of the bone matrix-like collagen. By collection of the electrospun core-shell nanofibers onto a high-speed rotating mandrel, aligned nanofiber matrices were obtained. Subsequently, hBMSCs were seeded onto the aligned nanofiber matrices. As expected, such aligned fibers supported the elongation of hBMSCs and the expression of Col I while inhibiting cell proliferation. Then, the cell-laden matrices were L-b-L stacked to form the 3D lamellae assembly (LA). Considering that the angles of 30 and 60° are close to 45°, we thus selected 0 and 45° as the representative ones of overlapped lamellae to further investigate the effect of superimposing angles on the osteogenesis of hBMSCs. During the assembly, two superimposing angles of 0° (LA-AF-0) and 45°(LA-AF-45) were chosen to represent the organization scenarios of natural bone matrix fibers. The LA with random core-shell nanofibers (LA-RF) was also similarly prepared as a control. Upon further culture, the hBMSC-populated assemblies were analyzed for osteogenic differentiation and mineralization. Interestingly, hBMSCs in both LA-AF-0 and LA-AF-45 assemblies underwent noticeable osteogenic differentiation (i.e., upregulation of RUNX2, OPN, and OCN); however, more pronounced induction was seen with LA-AF-0 in terms of elevated osteogenic marker expression (e.g., OCN and OPN) and mineralization (calcium deposition). Further analyses revealed that hBMSCs in the LA-AF-0 assembly showed an increase in not only total integrin $\beta 1$ but also in the phosphorylated ones (activated integrin β 1). Furthermore, such an activation triggered the focal adhesion kinase (FAK) extracellular regulated kinase 1/2 (ERK1/2) mitogen-activated protein kinase (MAPK) cascade, which in turn upregulated those osteogenic marker genes and mineralization for bonelike tissue formation. The findings suggest that the superimposing angles of the lamellae assembly would impact the osteogenic differentiation of hBMSCs, which can serve as the guidance toward hBMSC-assisted bone tissue engineering and provide an in vitro model to understand the effects of the bonelike matrix and configurations on cellular functions of boneforming cells.

2. MATERIALS AND METHODS

2.1. Materials. Poly(epsilon-caprolactone) (PCL, MW = 80 000), α -MEM, insulin-like growth factor (IGF), and basic fibroblast growth factor (bFGF) were purchased from Gibco (Grand Island, NY), and ascorbic acid and β -glycerophosphate were purchased from Sigma-Aldrich (St. Louis, MO). 1,1,1,1,3,3,3-Hexafluoro-2-propanol (HFIP) was obtained from Oakwood Products Inc. (West Columbia, SC). Bovine calf skin type I collagen (Col I) was purchased from Elastin Products Co. (Owensville, MO). Fetal bovine serum (FBS) was purchased from the American Type Culture Collection (ATCC, Manassas, VA). All other reagents and solutions were obtained from Thermo Fisher Scientific (Carlsbad, CA) unless indicated and were used as received.

2.2. Fabrication and Characterizations of Core-Shell Nanofibers. To fabricate the core-shell nanofibers, a coaxial electrostatic spinning device (Figure 1a) similarly described somewhere else 11 was used. Briefly, one 3 mL syringe containing a PCL/ Col I (v:v = 3:1) mixture of PCL (8% (w/v) in HFIP) and Col I (8% (w/v) in HFIP) was connected to the stainless-steel coaxial needle ① with an inner diameter of 0.64 mm. Another 3 mL syringe containing only Col I (8% (w/v) in HFIP) was connected to needle ② with an

inner diameter of 1.48 mm. Upon insertion of needle ① (core) through needle ② (shell), the coaxial electrostatic spinning device was connected to a dual-channel syringe pump, and the tips of coaxial needles were connected to the high-power supply. Under the optimized conditions (15 kV (voltage), 10 μ L/min (extrusion speed), 4 °C (temperature), and 75% (humidity)), the core-shell nanofibers were collected onto the paper rings (outer diameter: 20 mm; inner diameter: 15 mm) attached onto either a grounded copper plate to obtain randomly oriented nanofiber matrices (called RF) or a grounded rotating mandrel ($\emptyset = 10 \text{ cm}$) with tunable rotating speeds (1000, 2000, or 3000 rpm) to obtain aligned nanofiber matrices (called AF). To obtain PCL/Col I-only nanofibers, needle ② alone was connected to a syringe with a PCL/Col I (v:v = 3:1) mixture and electrospun under the same above-mentioned conditions. For all cases, the fibers were collected for 5 min and then kept in a vacuum oven for 24 h to remove the residue of HFIP.

To confirm the presence of the core structure within the core-shell nanofibers, the nanofibers collected onto a carbonized copper grid were observed using a transmission electron microscope (TEM, JEOL, Japan) at 100 kV. To determine the diameter and organization of electrospun nanofibers, the collected fibers were sputter-coated with gold and then examined with a scanning electron microscope (SEM, Ultra-55, Zeiss, Germany) at an accelerating voltage of 15 kV. To determine the morphological features of collagen on the surface of core-shell nanofibers, the collected nanofibers were profiled with an atomic force microscope (AFM, Bioscope Catalyst Nanoscope-V, Veeco Instruments, Plainview, NY).

To determine the stability of core-shell nanofibers, the as-prepared nanofiber matrices were incubated in phosphate-buffered saline (PBS, pH 7.4) at 37 °C. At designated times, the matrices were harvested, gently rinsed with deionized (DI) water, lyophilized, and examined by TEM. In order to further investigate the behaviors of core—shell fibers in vivo, L-b-L stacked multilayer discs (50 layers, 5 mm in diameter) of PCL/Col core fibers or core-shell nanofibers were subcutaneously implanted in C57BL/6J mice (6 weeks old) obtained from Guangdong Yaokang Biotechnology Co., Ltd. At 4 and 8 weeks, the mice were sacrificed and the tissue with implanted fibrous discs were harvested. Upon fixation and dehydration, the embedded tissue specimens were cut into thin sections and stained with hematoxylin and eosin (H&E) for analyzing the in vivo degradation. All animal experiments were performed in accordance with the guidelines evaluated and approved by the Ethics Committee of Jinan University.

2.3. Cell Culture. Primary human bone marrow mesenchymal stem cells (hBMSCs, passage 1) purchased from the ATCC were cultured in the proliferation media composed of 10% FBS, 89% α -MEM basal medium containing 125 pg/mL bFGF, 15 ng/mL IGF, and 2.4 mM L-glutamine, and 1% penicillin-streptomycin (BI, USA, 10 000 U/mL-10 mg/mL) for expansion. Upon reaching 60-70% confluence, cells were trypsinized with 0.25% trypsin-EDTA and subcultured at a split ratio of 1-3.

2.4. Culture of hBMSCs on Core-Shell Nanofibers with Varying Fiber Organization. 2.4.1. Cell Seeding and Culture. Upon sterilization under a UV light for 30 min on each side, the fiber membranes were placed in 6-well plates and incubated with the proliferation culture media (the same as in Section 2.3) overnight prior to use. hBMSCs (passage 2-4) suspended in 2 mL of proliferation media were added to the wells at a density of 1×10^5 cells/well. The cells were cultured at 37 °C, 5% CO₂, and 95% humidity for designated periods with the media refreshed every other

2.4.2. Cell Adhesion and Proliferation. After cell seeding, the control (tissue culture plastic), RF-hBMSCs, and AF-hBMSCs were gently rinsed with PBS (pH 7.4) at 3 and 6 h, respectively. The cell counting kit-8 (CCK-8, Sigma) was utilized to assess the number of cells attached to the matrices in order to determine the cell adhesion efficiency in comparison to the tissue culture plastic surface. Cell proliferation was determined by measuring the metabolic activity using the Titer Blue assay following the manufacturer's protocol. Briefly, upon culture for 3, 5, 7, and 9 days, 800 μ L of the Titer Blue working solution was added to each well and incubated for 2 h in the

dark. 100 μ L of the supernatant was transferred to the 96-well plates, and the fluorescence absorbance at 560/590 nm was measured using the BioTek Synergy H1 hybrid multimode reader (Agilent Technologies, Inc., Santa Clara, CA).

2.4.3. Immunofluorescence Staining. Cells cultured on various substrates for 3, 5, 7, and 9 days were fixed in 4% paraformaldehyde for 10 min, rinsed 3 times with phosphate-buffered saline (PBS), and permeabilized with 0.1% Triton-100 for 10 min. After rinsing with PBS, 200 µL of rhodamine-conjugated phalloidin (Sigma, 1:200) was added to each well, and the wells were incubated in the dark for 30 min at room temperature. Cell nuclei were counterstained with DAPI for 10 min. The stained cultures were examined using a BioTek Cytation C10 confocal imaging reader (Agilent Technologies, Inc.). Fluorescence images were analyzed using ZEN core and ImageJ 1.52 (NIH) to characterize the cell morphology.

Besides cell morphology, the cells cultured for 7 and 14 days were also immunofluorescently stained for Col I. Briefly, the fixed cultures were blocked with 1% BSA in PBS for 1 h to prevent nonspecific protein interactions. Upon blocking, the cultures were incubated with the primary rabbit antihuman Col I antibody (1:500 dilution in 1% BSA) overnight at 4 °C. After washing with PBS twice, the cultures were incubated in the dark with the secondary antibody (Alexa Fluor 647-conjugated donkey antirabbit IgG H&L) (1:500 dilution in 1% BSA) for 1 h at room temperature. Cell nuclei were stained with DAPI for 10 min. The stained samples were visualized with the BioTek Cytation C10 confocal imaging reader, and the images were analyzed using ZEN core and ImageJ.

2.5. Layering of Cell-Seeded Nanofiber Matrices. To emulate the lamellae organization of the natural bone matrix, L-b-L stacking was used to assemble the cell-seeded nanofiber matrices into 3D constructs. 12 Briefly, hBMSCs were seeded onto nanofiber matrices at a density of 1×10^5 cells/membrane. After incubation for 30 min, five layers of cell-seeded matrices were overlaid on top of each other (Figure 1) and immobilized with the aid of a pair of customized stainless-steel (SS) rings (Figure S1, Supporting Information). These rings were designed with a meshed grid in the middle to support the cell-seeded fiber matrices and a tapered edge for easy assembly. During the L-b-L assembly, the first SS ring was placed in the culture medium, followed by the stacking of hBMSC-loaded RF or AF matrices at a predetermined angle on it. Subsequently, a second SS ring was placed on top and gently pressed to interlock with the first ring, securing the assembled matrices. Three types of lamellae-like cell/nanofiber-assembled constructs were configured. The assembled constructs prepared from hBMSC-seeded RF matrices were called LA-RF. The assembled constructs prepared from hBMSC-seeded AF matrices were named LA-AF-0 with the overlay angle of 0° or LA-AF-45 with the overlay angle of 45°. The assembled constructs were further cultured for designated time periods. The medium was refreshed every other day.

To better visualize cell distribution within the layered constructs, hBMSC-seeded AF after culture for 1 day was fixed and was fluorescently stained with Alexa Fluor 488(green)- or Alexa Fluor 647(red)-conjugated phalloidin (Waltham, MA). Following the stacking order (in alternate fluorescence), hBMSC-seeded AF was, respectively, assembled into three-layer constructs with the designated overlay angle (45 or 0°). The assembled constructs were then examined by using the BioTek Cytation C10 confocal imaging reader.

2.6. Characterization of hBMSC Osteogenic Differentiation within Layered Constructs. 2.6.1. Histological Analysis. Layered constructs (LA-AF-0 and LA-AF-45) cultured for 7 and 14 days were fixed in 4% paraformaldehyde and then processed for dehydration with a series of graded ethanol solutions until 100% ethanol. The dehydrated samples were embedded and sectioned into thin sections $(4-7 \mu m)$. The sections were then stained with hematoxylin and eosin (H&E) for cell distribution and morphology or Masson staining for the new extracellular matrix. The stained sections were examined under a 80i Nikon microscope and representative images were recorded.

2.6.2. Real-Time PCR. To determine the osteogenic differentiation of hBMSCs within the layered 3D constructs, gene expression of

selected osteogenic markers for early differentiation (runt-related transcription factor (RUNX2), Col I, and ALP) and late differentiation [osteopontin (OPN) and osteocalcin (OCN)] was studied using the real-time polymerase chain reaction (RT-PCR) at days 1, 3, and 7. To address how nanofiber alignment induced an early cellular response (i.e., 1 and 8 h), gene expression of integrins α 2, α 3, and β 1 was also studied. Briefly, total RNA (n = 3) was isolated using the Multisource Total RNA Miniprep Kit (AxyPrep Biosciences, Union City, CA). RNA was reverse-transcribed into complementary DNA (cDNA) using the SuperScript First-Strand Synthesis System (Promega, Fitchburg, WI) and cDNA was then amplified using recombinant Taq DNA polymerase (Promega). cDNA was amplified by using primers of Col I, OPN, OCN, RUNX2, and integrins α 2, α 3, and β 1, and GAPDH served as the housekeeping gene (see Table S1, Supporting Information) (Invitrogen, Carlsbad, CA). Amplified genes were quantified based on the fluorescence. The relative mRNA expression was normalized based on $2^{-\Delta\Delta Ct}$ ($\Delta Ct = Ct$ (target gene) - Ct (reference gene), $\Delta\Delta$ Ct = Δ Ct (experimental group) - Δ Ct (control group)).

2.6.3. Western Blot Analysis. To determine the expression of targeted proteins, the culture was analyzed with Western blot. Briefly, after culture for 21 days, hBMSCs from LA-RF, LA-AF-0, and LA-AF-45 cultures were collected and centrifuged for 10 min at 1500 rpm. After washing with PBS twice, the cells were lysed in 50 μ L of RIPA buffer (containing the protease inhibitor PMSF) on ice and vortexed for 5 min. Upon complete lysis, the lysates were centrifuged at 14 000 rpm for 15 min and the supernatants were transferred to the precooled tubes. The collected protein samples were transferred onto a poly(vinylidene difluoride) membrane (PVDF, Millipore-IPVH00010, Sigma), which was then blocked with 5% skim-milk solution. The blocked membrane was then respectively incubated with primary antibodies (Col I, OPN, OCN, ITGA α 2, ITGA α 3, ITGA β 1, HUTS-4, FAK, phospho-FAK (p-FAK), ERK1/2, phospho-ERK1/2 (p-ERK1/2), and GAPDH). All primary antibodies except GAPDH (Santa Cruz Biotechnology, Santa Cruz, CA) were purchased from Thermo Fisher. Afterward, the membranes were washed 3 times with 1 × TBST and then incubated with the secondary antibody (H&L Alexa Fluor 64-conjugated polyclonal goatantirabbit IgG) (ab150079, Cambridge, MA). The blots were then imaged using the Bio-RAD ChemiDoc XRS imaging system (Hercules, CA).

2.6.4. Alizarin Red Staining for Calcium Deposition. To better characterize the osteogenic differentiation of hBMSCs, mineral deposition was determined by staining calcium with alizarin red. Briefly, hBMSCs within LA-RF, LA-AF-0, and LA-AF-45 were cultured 7, 14, and 21 days in complete media supplemented with 10 mM β -glycerophosphate, 10^{-7} M dexamethasone, and 80 μ g/mL ascorbic acid. The cultures were stained with 2% alizarin red in 0.05 M Tris-HCl (pH = 4.2) for 10 min and then washed with D.I. water prior to photographing. Subsequently, 1% hexadecane pyridine chloride was added to the stained cultures to extract the stain. The extracts were then transferred to a 96-well plate to measure the absorbance at 462 nm for quantitative analysis of the calcium amount.

2.6.5. X-ray Diffraction (XRD) for the Crystalline Components in Cell Mineralization. The crystal composition of the samples was determined by X-ray diffraction (XRD, MSAL XD-2×, Blige Technology Co., Ltd.) at a voltage of 36 kV, a tube flow of 20 mA, a Cu K α radiation source, and a scanning range (2 θ) of 5-60°.

2.6.6. Mechanical Testing. LA-RF, LA-AF-0, and LA-AF-45 cultured up to 7 and 21 days were tested for their mechanical performance by using a universal tension machine (BioDynamic 5010). Cell-free scaffolds incubated in the culture medium for 7 days were included as controls. The crosshead speed is 1 mm/min.

2.7. Mechanistic Understanding of Osteogenic Differentiation of hBMSCs within Layered Constructs. To further determine the regulatory mechanism on the osteogenic differentiation of hBMSCs within the lamellae-like assembly, expression of integrins α 2, α 3, and β 1 and GAPDH genes at day 7, 14, and 21 was studied by using real-time PCR, as shown in Section 2.6.2. cDNA was amplified

using the corresponding primers (Invitrogen, Waltham, MA), as listed in Table S1 (Supporting Information).

To further confirm the occurrence of integrin $\beta 1$ activation to hBMSCs within the layered constructs, immunofluorescence staining for phosphorylated integrin $\beta 1$ was also performed by the respective incubation with the antibody against the active conformation of $\beta 1$ integrin (Millipore, clone HUTS-4, 1:300) and the goat antimouse IgG-FITC conjugate secondary antibody (Caltag, PAB4971, 1:400). Stained samples were examined with a C10 confocal imaging reader.

Upon culture for 21 days, hBMSCs cultured within the LA-RF or LA-AF-0/45 assembly were lysed and Western blot analysis was performed. The blots transferred to the PVDF membrane were blocked with 5% skim-milk and then incubated with the corresponding antibodies against ITGA α 2, ITGA α 3, ITGA β 1, phospho-ITGA β 1 (HUTS-4), FAK, phospho-FAK (p-FAK), ERK1/ 2, phospho-ERK1/2 (p-ERK1/2), and GAPDH. To further confirm the involvement of ITGA β 1 in overlay angle-induced signal transduction, hBMSCs in the LA-AF-0/45 assembly were treated with 10 μ M GLPG0187¹³ (G0187, antagonist for ITGA β 1, MedChemExpress LLC, Monmouth Junction, NJ). We also treated the cultures with 10 μ M U0126, a blocker of ERK1/2 phosphorylation, to determine the involvement of ERK1/2 in the overlay angleinduced osteogenic differentiation of hBMSCs.

2.8. Statistical Analysis. Experiments were repeated at least three times, and statistical analyses were performed using analysis of variance (one-way ANOVA) or Tukey's test. The P value less than 0.05 was considered significant and otherwise considered nonsignificant (ns).

3. RESULTS AND DISCUSSION

3.1. Fabrication of Lamellae-like Matrices with Core-**Shell Nanofibers.** With the use of the coaxial electrospinning setup (Figure 1a), core-shell fibers were successfully obtained. TEM examination of the as-prepared fibers revealed the coreshell structure, i.e., the dark core and the light shell (Figure 1b). Based on TEM images, the average thickness of the Col I shell was 78.7 ± 7.5 nm, while the diameter of the PCL/Col I core was 182.4 ± 8.2 nm. Actually, both the shell thickness and the core diameter are tunable, which are closely correlated with several key parameters, including the concentration of each solution, the feeding rate of each solution, the diameter of coaxial needles, the electrical field intensity, and the collecting distances between needle tips and the collecting surface. The fiber diameter chosen for this study was solely benchmarked to the typical bone matrix fibers, which are in the diameter range of 30-500 nm. 14 The surface features of core-shell fibers were also characterized by using AFM. Compared to the relatively smooth PCL/Col I fiber (Ra = 0.46 ± 0.12 nm), the Col I shell was rougher (Ra = 2.17 ± 0.32 nm) with noticeable nanosized bumps (see Figure 1b, arrows). We believe that during the electrospinning, the combination of rapid volatilization of HFIP and high electric field-induced shear stress would facilitate the self-assembly of Col I into fibril structures, accounting for the increased roughness and the formation of those nanosized bumps. In particular, studies have elucidated that unidirectional stress could drive the self-assembly of collagen molecules to form periodic structures. 15 Interestingly, the nanosized patterns of the Col I shell were elongated following the longitudinal direction of core-shell nanofibers. It is necessary to mention that the inclusion of PCL in the core provides both mechanical strength and structural stability to the electrospun fibers, which cannot be achieved with pure collagen. As shown in Figure S3 (Supporting Information), the Col I shell of the core-shell nanofibers became invisible after incubation in PBS for 7 days (Figure S3B, Supporting

Information), while the PCL/Col I core retained its morphological stability even after 14 days (Figure S3C, Supporting Information). Col I in the shell not only provides the adhesive motifs to cells for desirable adhesion but also presents the topological nanofeatures close to the natural collagen fibers of the bone matrix. 15 Clearly, such delicate attributes were not seen with electrospun polyblend PCL/Col I fibers, further implying the benefits of the core-shell nanofibers. Implantation of the layered core-shell nanofibrous matrices in the subcutaneous pockets of mice showed that the matrices became folded (Figure S4, Supporting Information) and were readily visualized within 4 weeks. Based on the in vitro degradation study, the Col I shell of the core-shell nanofibers by this time might be completely degraded, and the remaining fibers were probably mainly composed of PCL/Col I core fibers. By week 8, even hard-to-degrade PCL within the PCL/Col I fibers underwent degradation, leading to a structural breakdown (Figure S4, Supporting Information). Previous studies demonstrate that by this time, substantial new bone formation would occur during in situ bone regeneration, 15 and timely degradation of PCL/Col I fibers could offer the required space for the new bone tissue.

Organization of the electrospun core-shell fibers within the collected matrices is closely regulated by the way the fibers are collected. ¹⁶ In this study, the fibers were collected onto either grounded stationary copper plates or a grounded rotating mandrel at different rotating speeds. As noted, the fibers collected on a stationary surface exhibited a randomly arranged organization, which most likely results from the whipping effect of the electrospinning jet. However, the fibers collected onto a rotating mandrel showed a preferred orientation following the rotating direction of the mandrel, and it became much more pronounced with a higher rotating speed (e.g., 2000 rpm) (Figure 1c). To better correlate the fiber organization with the rotating speed, SEM images of the obtained fiber matrices at different speeds were analyzed by using the Nightingale rose diagram. As shown in Figure 1c, when the rotating speed reached 3000 rpm, up to 88% of the core-shell nanofibers were oriented within 10° of the mandrel rotating direction. The orientation might primarily result from the shear force generated by the rotating mandrel, which induces the stretch of the electrospun fibers in the direction of mandrel rotation. As a consequence of stretching, the average fiber diameter should decrease over the rotating speed, as well. Indeed, the average diameter of the fibers at 1000 rpm was 357.6 \pm 93.3 nm and then decreased to 260.1 \pm 55.4 nm (2000 rpm) and 215.5 \pm 41.3 nm (3000 rpm), respectively. For the remaining studies, electrospun fiber matrices at 3000 rpm were used. For convenience, we referred the fiber matrices collected at 3000 rpm to aligned fiber (AF) matrices, and those collected on the stationary surface as random fiber (RF) matrices (Figure S2, Supporting Information).

3.2. Osteogenic Differentiation of hBMSCs Cultured on AF Lamellae-like Matrices. Our previous study together with others has shown that aligned electrospun nanofibers would induce the osteogenic differentiation of preosteoblasts.¹⁰ However, it is unclear whether such observations could similarly occur to hBMSCs cultured on the core-shell nanofibers. Thus, hBMSCs seeded and cultured on AF or RF core-shell nanofibers were studied for their osteogenic differentiation. To confirm the support of cell adhesion by core-shell nanofibers, hBMSCs were seeded onto the matrices and analyzed for the cell adhesion rate in comparison to the

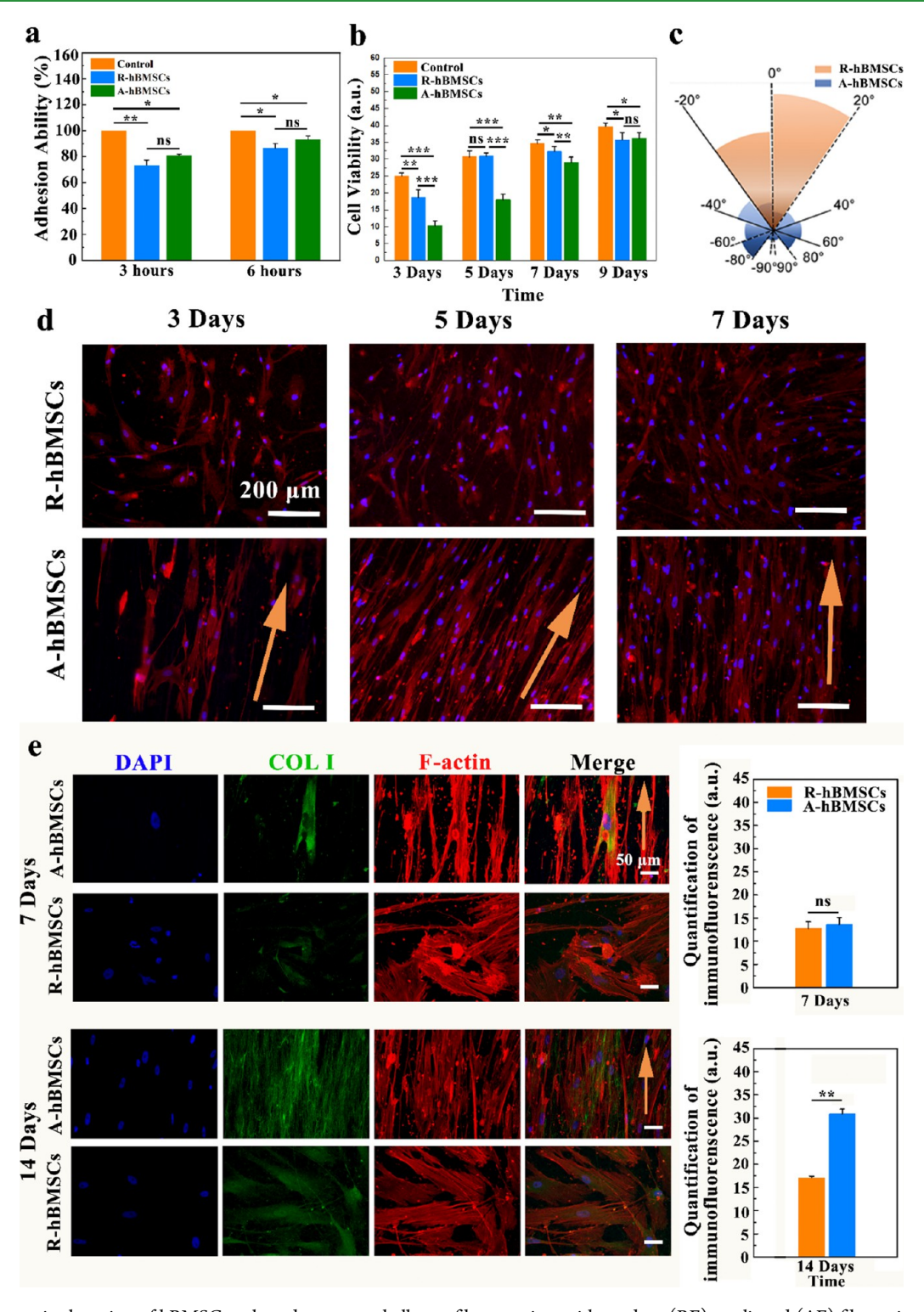


Figure 2. Phenotypic alteration of hBMSCs cultured on core—shell nanofiber matrices with random (RF) or aligned (AF) fiber orientation, defined as R-hBMSCs and A-hBMSCs, respectively. (a) Cell adhesion onto RF and AF after culture for 3 and 6 h and cells were determined by CCK-8 assay. (b) Cell proliferation of R-hBMSCs and A-hBMSCs (n=3), in which the cell metabolic activities were determined by MTS assay. (c) Nightingale rose plot of the cell orientation angle of R-hBMSCs and A-hBMSCs, in which the orientation angles were quantified based on the fluorescence images (n=5) in panel (d). (d) Representative fluorescence images of the morphology of R-hBMSCs and A-hBMSCs after culture for 3, 5, and 7 days. The cells were stained for F-actin (red) with rhodamine-conjugated phalloidin, and nuclei were stained blue with DAPI. The arrow indicates the orientation of AF. (e) Representative immunofluorescence images of R-hBMSCs and A-hBMSCs cultured for 7 and 14 days for Col I (green), F-actin (red), and cell nuclei (blue). Semiquantification of the green fluorescence intensity by using ImageJ. *p < 0.05; **p < 0.01; ***p < 0.001, ns = not significant.

tissue culture plastic surface. As shown in Figure 2a, both RF and AF matrices supported cell adhesion in a similar manner,

i.e., more cells attached upon prolonging the incubation time from 3 to 6 h and achieved more than 80% by 6 h. Notably,

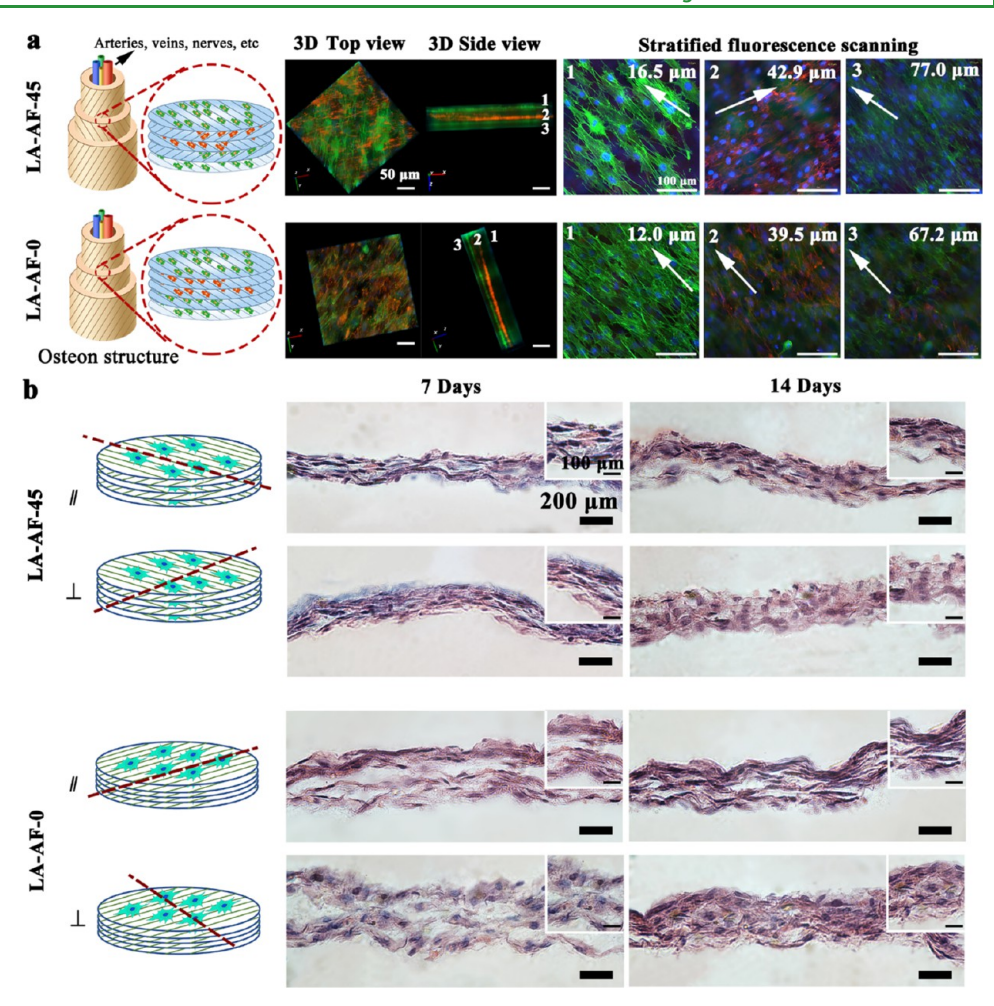


Figure 3. Distinct cell organization within the 3D assembly of cell-laden fibers. (a) Confocal fluorescence images of LA-AF-45/0 constructs after the L-b-L assembly, in which green fluorescence-labeled cells are located in the upper and bottom layers, while red fluorescence-labeled cells are in the middle layer (middle) following the schematic illustration (left). Z-scanned images (right) showed the distinct cell orientation from layer to layer depending on the overlay angle. (b) Representative microscopic images of LA-AF-45/0 constructs, in which cross-sections following the indicated sectioning directions were stained with H&E for the cell nuclei (blue) and cytoplasm (pink). Inset: zoom-in images of the selected area. Depending on the overlay angle and sectioning direction, cell nuclei exhibited different shapes and varying aspect ratios.

slightly more cells adhered to AF matrices compared to RF ones, although there was no discernible difference. Interestingly, both AF and RF matrices supported continuous proliferation of hBMSCs; however, a lower cell proliferation rate was seen on the AF matrices in comparison to RF matrices or the tissue culture plastic (TCP) surface as controls, particularly in the early time points (3, 5, and 7 days) (Figure 2b), which seems contradictory to the cell adhesion results. Both AF and RF matrices supported the attachment and spreading of hBMSCs, but they induced a distinct cell morphology (Figure 2c,d), i.e., cells on AF matrices displayed an elongated and much slender morphology following the same direction of fiber alignment, while on RF matrices, cells were randomly distributed without a noticeable orientation and less elongation. To better characterize the cell orientation, we also performed cell orientation angle analysis, i.e., the long axis of cells relative to the fiber alignment, and developed the Nightingale rose diagram (Figure 2c). As expected, the cell orientation angle on AF matrices was within ±20° from the fiber alignment, very similar to the cell arrangement in the bone matrix.¹⁷ This feature was not found with the cells on the RF matrices. It is well established that cell morphology is significantly regulated by the topology of substrate surfaces via

contact guidance.¹⁸ And such a distinct morphology on AF matrices was retained for all investigating time points (3, 5, and 7 days). Such a disparity may result from two possible reasons: (1) the adhered cells need to adapt to the new environment before an active growth phase (nanofibers vs TCP surface) and (2) the commitment of those cells adhered on AF toward osteogenic differentiation delays the proliferation (AF vs RF). As indicated in the early finding, the time-resolved metabolic activities of differentiated stem cells fluctuate continuously.¹⁹ Furthermore, upon reaching the confluence, the stem cells would pivot more toward differentiation. As a result, cells exhibit reduced proliferation particularly in the prolonged culture phase while promoting the synthesis of the extracellular matrix for mineralization.²⁰ Thus, AF matrices might favor the osteogenic differentiation of hBMSCs. Immunofluorescence staining for Col I was performed on the culture from both days 7 and 14. Although no obvious difference was recognized in Col I staining of cells cultured on AF and RF matrices on day 7, an elevated Col I fluorescence was seen with the cells cultured on AF matrices by 14 days (Figure 2e). Semiquantification of the fluorescence intensity did confirm that there was a significant difference in Col I expression by hBMSCs on RF and AF matrices (p < 0.01). The results

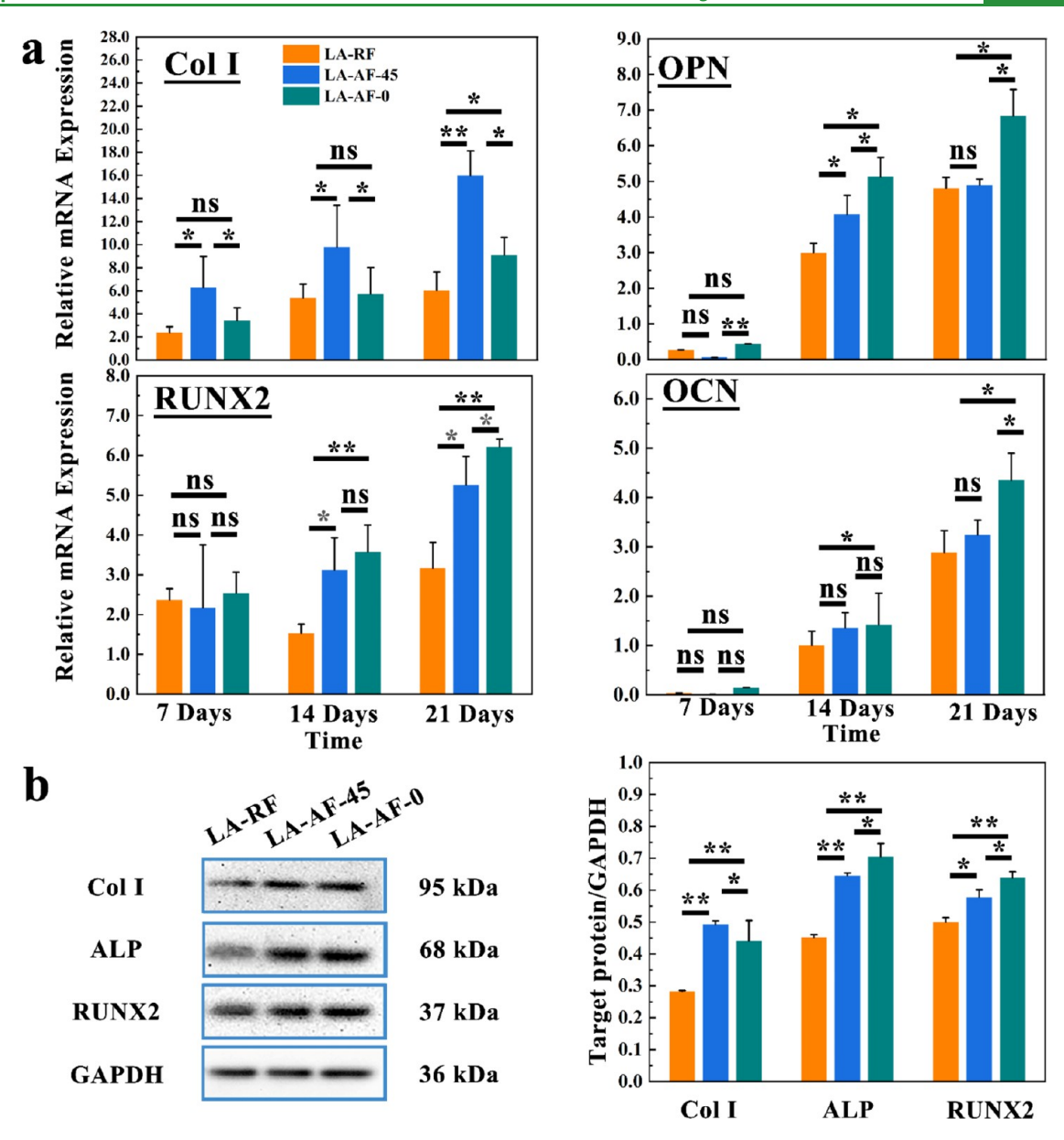


Figure 4. Expression of osteogenic markers of hBMSCs within the 3D assembly of cell-laden fibers. (a) Expression of osteogenic differentiation marker genes of Col I, RUNX2, OPN, and OCN in hBMSCs as measured by real-time PCR. Cells on the tissue culture plastic surface serve as controls. (b) The proein level of selected osteogenic markers (Col I, RUNX2, ALP) was analyzed via Western blot. The representative blot image was shown on the left and semiquantification was shown on the right. *p < 0.05, **p < 0.01, ns: nonsignificant.

suggest that AF-induced elongation of hBMSCs favors the synthesis of Col I in hBMSCs, which is consistent with previous findings that directional organization prompts hBMSCs to produce more collagen.²¹ As a matter of fact, Col I synthesis is the basic step toward the rebuilding of the bone matrix, which sequentially serves as the substrate for mineralization occurring during cell differentiation and new bone formation.²²

3.3. Assembly of Cell-Laden Lamellae-like Matrices to Form 3D Layered Constructs. Previously, we have shown the possibility of stacking cell-seeded fiber matrices in a L-b-L manner to form 3D constructs. During the stacking, it is flexible to adjust the overlay angles from layer to layer (Figures S1 and S5 in the Supporting Information). Thus, two representative overlay angles (0 and 45°) were particularly chosen. Following the procedures illustrated in Figure 3a, cell-laden AF matrices (16.4 \pm 2.2 μ m thick) were stacked into 3D

constructs with two configurations, namely, LA-AF-45 (overlay angle: 45°) and LA-AF-0 (overlay angle: 0°). To better visualize the spatial organization of cells within the assembled constructs, hBMSCs, respectively, labeled in red or green fluorescence were seeded onto AF matrices prior to stacking. The top view revealed the presence of both red and green cells in the assembled constructs, while the side view clearly showed the alternation of red and green cell layers (Figure 3a top view and Videos S1 and S2, Supporting Information). As the cells elongated along the same direction of the fiber alignment, the rotation angle of the cell orientation between cell layers could be used to indicate the overlay angles of stacking. As revealed by the Z-scanning images, the angle between oriented green and red cells in LA-AF-45 was close to 45°, while those cells in LA-AF-0 were in parallel (Figure 3b and Videos S1 and S2, Supporting Information). Taken together, the above results confirm that the L-b-L assembly of cell-laden AF can effectively

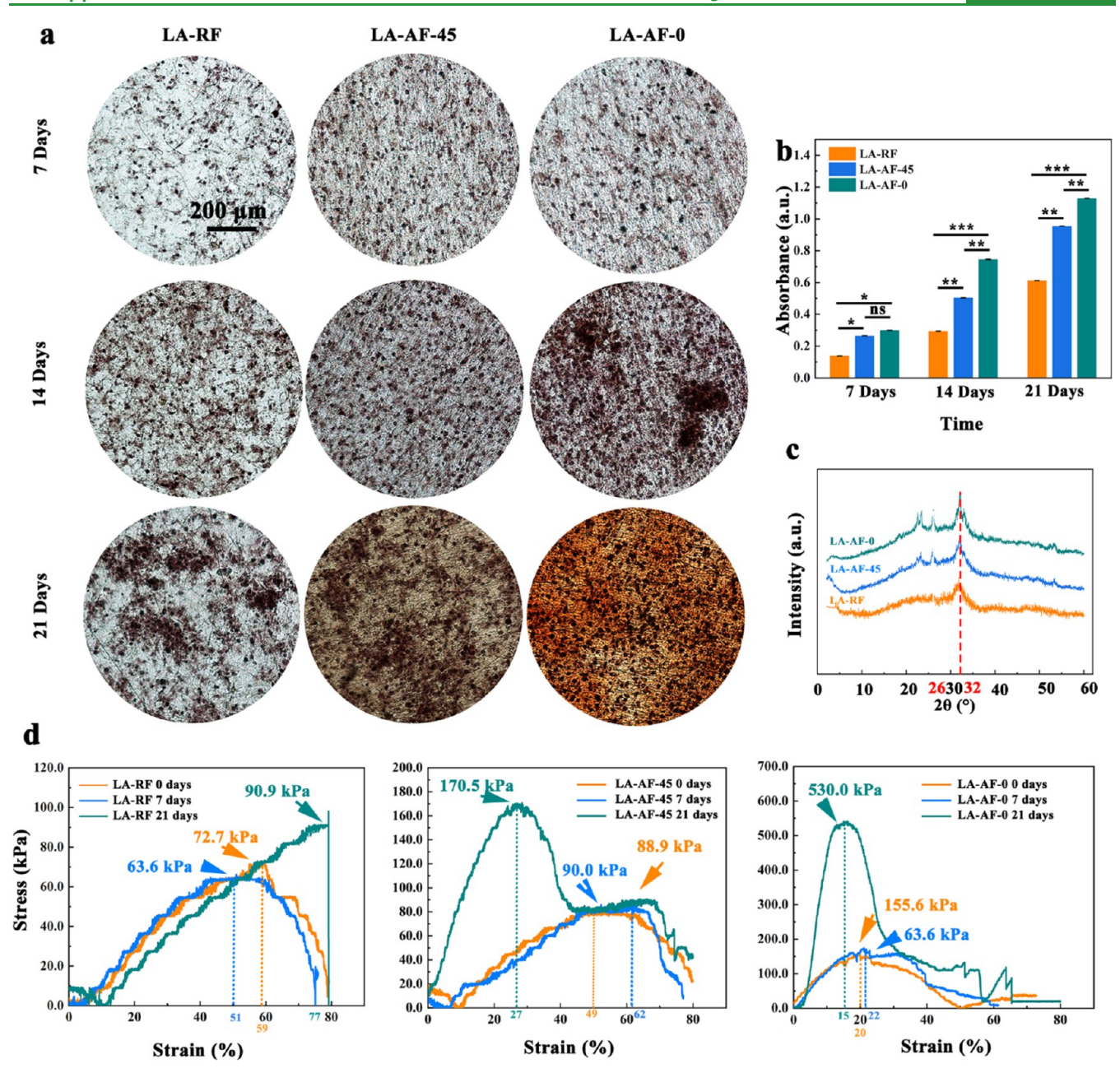


Figure 5. Time-resolved mineralization of the 3D assembly of cell-laden fibers. (a) Optical images of LA-RF and LA-AF-0/45 assemblies stained with alizarin red on days 7, 14, and 21. (b) Quantitative analysis of alizarin red-stained cultures. (c) XRD patterns of the mineralized cultures for 21 days. (d) Representative stress—strain curves of wet-state LA-RF and LA-AF-0/45 specimens cultured for 0, 7, and 21 days, as determined by tensile testing (n = 4).

form multilayered constructs with fiber organization similar to those ECM lamellae of the native bone. More importantly, the cells in the assembled constructs closely followed the AF organization, allowing to further investigate the effects of the overlay angle on the BMSC osteogenic differentiation.

To further determine whether hBMSCs within the assembled cell-laden AF constructs retained their spatial distribution and morphological orientation upon prolonged culture, the constructs cultured for 7 and 14 days were cut into thin cross-sections in the designated direction and then subjected to H&E staining. As shown in Figure 3b, the cells evenly distributed across the assembled layers within both 7-and 14-day LA-AF-0 constructs; however, the cell nuclei showed a distinct morphology depending on the sectioning

direction: in parallel sections (//), the cell nuclei exhibited an elongated shape following AF orientation, while in perpendicular sections (⊥), the cell nuclei were mostly round. This observation is consistent with the initial cell morphology, as shown in Figure 3a, confirming that cells in LA-AF-0 retained the substrate-guided cell orientation even after cultivation for 14 days. On the other hand, in both perpendicular and parallel sections of LA-AF-45, the cell nuclei appeared to be a mixture of round and elongated ones, which most likely result from the cross alignment of AF matrices and consequently offset partially the substrate-induced elongation effect. It is necessary to mention that the extended culture favored the formation of the packed structure, i.e., loosely assembled cell-laden AF matrices (1-week culture) vs densely packed cell-laden AF

constructs (2-week culture), which was similarly observed for both LA-AF-0 and LA-AF-45 assemblies, but more pronounced with LA-AF-0. The time-dependent formation of such packed structures might be due to the newly deposited ECM proteins, which glue the cell-laden AF matrices together. Taken together, the above-observed results suggest that the L-b-L assembly of cell-laden AF matrices would allow to form bone lamellae-like tissue constructs while providing continuous morphological regulation to the encapsulated cells via contact guidance with surrounding AF.

3.4. Effect of the Overlay Angle on the Osteogenic Differentiation of hBMSCs within 3D Layered Con**structs.** To determine whether the overlay angles (0 and 45°) of cell-laden AF within LA-AF constructs affect the osteogenic differentiation of hBMSCs, gene and protein expressions of selected osteogenic markers were analyzed on the cultured LA-AF constructs. Real-time PCR analysis showed that (Figure 4) upregulated Col I gene expression was seen with hBMSCs in LA-AF-45 as early as 1 week compared to those from other culture conditions (LA-RF: the L-b-L assembly of cell-laden RF; LA-AF-0) and became more pronounced at weeks 2 and 3 (Figure 4). Compared to the LA-RF group, elevated Col I gene expression was also seen with the LA-AF-0 group, but only at week 3 and lower than the LA-AF-45 group. This suggests that aligned nanofibers would favor Col I gene expression even within the 3D assembly, similar to the circumstances on electrospun fiber surfaces, 17 while the overlay angles did induce differential responses. Interestingly, analysis of the ALP gene, a landmark of osteogenic differentiation, revealed a significantly higher expression in the LA-AF-0 group compared to other groups starting at week 2 (Figure S6, Supporting Information), implying that hBMSCs intersected in between parallel AF matrices (i.e., a 0° overlay angle) might be more favorable for osteogenic differentiation. Furthermore, as a key regulator of mineralization,²³ elevated ALP expression would also imply that the 3D lamellae assembly of LA-AF-0 seems to facilitate the onset of more mineralization.

Further analysis of RUNX2 and other osteogenic noncollagenous protein (NCP) (e.g., OCN and OPN) markers revealed that expression of these osteogenic genes was significantly higher in LA-AF-0 than in other groups at week 3, and such observations suggest that the LA-AF-0 assembly is more favorable to the residing hBMSCs for their osteogenic differentiation. Notably, OCN expression in LA-AF-0 and LA-AF-45 did not show an evident difference for the first 2 weeks, whereas RUNX2 and OPN, particularly OPN, already exhibited a higher expression in LA-AF-0 at week 2. As recognized, RUNX2 and OPN are considered the markers for pre- and premidstage osteogenic differentiation of stem cells, while OCN appears much later than both.²⁴

As cellular functions are directly regulated by the corresponding proteins, the protein level for selected osteogenic marker genes (i.e., Col I, ALP, OPN, OCN, and RUNX2) was analyzed by Western blotting. As shown in Figures 4b and S7 (Supporting Information), the elevated level of Col I, ALP, OPN, OCN, and RUNX2 was seen with both LA-AF-45/0 groups compared to the LA-RF cultures. To our surprise, the Col I protein level was statistically higher in LA-AF-45 compared to the other two groups. This result agrees with the recent findings that nanofibrous matrices with a random organization favor collagenous ECM secretion by MSCs²⁵ and the native bone matrix overlapping in angles tends to contain more collagen compared to those in the highly

aligned manner,²⁶ which can tolerate greater torsional and tensile forces with superior toughness, albeit with a lower degree of mineralization.²⁷ As expected, the LA-AF-0 group showed a higher expression of ALP and RUNX2 (p < 0.01) than the LA-AF-45 group. Both LA-AF-0/45 constructs showed a significantly higher level of OCN compared to LA-RF constructs, but between LA-AF-0/45, only slightly higher OPN and OCN were seen with LA-AF-0 (Figure S7, Supporting Information). These findings are consistent with real-time PCR results, further affirming that the overlay angle of 45° in the LA-AF assembly favors collagen synthesis and 0° overlaying is more conducive to the osteogenic differentiation of hBMSCs. Further investigation remains necessary to understand the mechanistic regulation of collagen synthesis by a 45° overlay angle.

Osteogenic differentiation of hBMSCs at the later stage would lead to biomineralization of the extracellular matrix, i.e., deposition of minerals onto the collagen matrix, an important indicator of the onset of bone formation.²⁸ Thus, various cellladen assemblies cultured for 7, 14, and 21 days were stained with alizarin red to visualize the deposition of calcium minerals. As shown in Figure 5a, compared to the LA-RF groups, LA-AF-0/45 showed noticeable calcium deposition by 14 days, and particularly LA-AF-0 constructs displayed the large calcium nodule formation. By 21 days, large calcium nodules also appeared in LA-RF constructs. However, enhanced calcium deposition was again observed in LA-AF-0 constructs, where rather homogeneous red calcium staining was clearly observed across the constructs compared to LA-RF or LA-AF-45 groups. Quantification of calcium deposition by measuring the absorbance of the extracts of stained calcium at 570 nm revealed a trend similar to the microscopic results, showing the highest measurement of the calcium extract with LA-AF-0 constructs for both 14 and 21 days (Figure 5b). To determine the mineralization composition, the constructs cultured for 21 days were examined with XRD. As shown in Figure 5c, no obvious crystalline peaks (except a negligible peak at 32°) were seen with hBMSCs cultured on the culture plastic surfaces, even with the osteogenic culture media (data not shown). While the crystalline peak at 32°, corresponding to the diffraction peaks of crystallographic features (112), (211), (300) of Hap, became more pronounced with LA-RF constructs, the representative peak at 26°, typically corresponding to the (002) crystallographic features [referring to the XRD standard card no. JCPDS 84-1998], was not noticeable. Distinct from LA-RF constructs, a crystalline peak at 26° was clearly observed with LA-AF-45 constructs despite its relatively low signals. To our surprise, the LA-AF-0 constructs exhibited strong crystalline peaks at both 26 and 32° for mature Hap, suggesting that the assembly of cell-laden AF matrices in a parallel fashion would better induce the osteogenic differentiation of hBMSCs and promote the deposition of mature Hap. This result is somewhat consistent with our previous observation with the preosteoblasts encapsulated within aligned PCL/Col I hybrid nanofibers, showing the presence of large mineral nodules after 21-day culture. The mechanical testing results (Figure 5d) revealed that among all of the constructs right after the assembly (no new ECM secretion), LA-RF showed the highest strain (59%) and LA-AF-0 showed the lowest strain (20%) while exhibiting the highest breaking stress (155.6 kPa), confirming the direct correlation of the overlay angle with the mechanical properties. With the cells continuously proliferated and differentiated, new

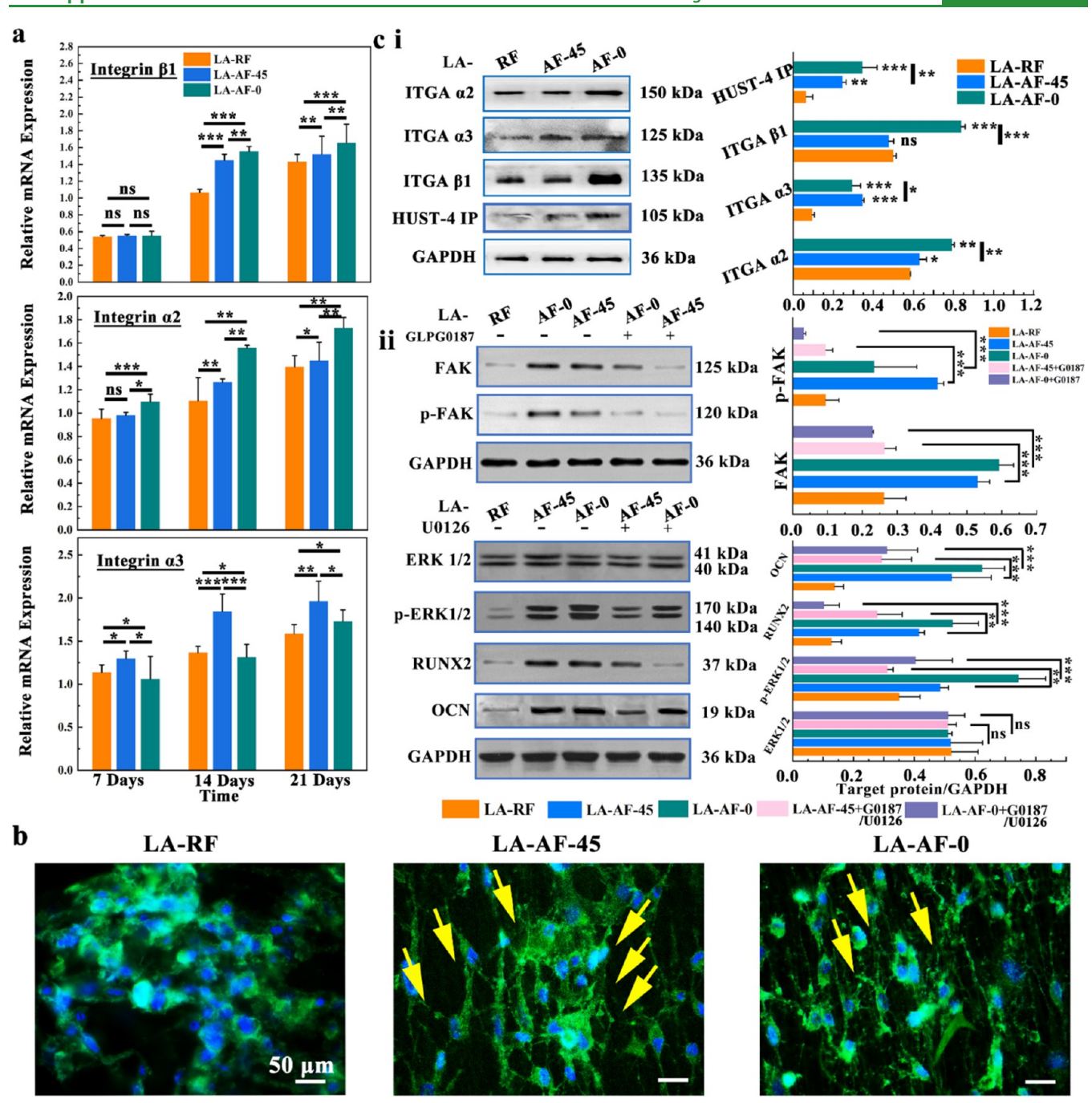


Figure 6. Expression of integrins β 1, α 2, α 3, and HUST-4 IP of hBMSCs within 3D cell-laden fiber assemblies. (a) Real-time PCR. (b) Immunofluorescence images of activated integrin β 1 (green). Yellow arrows indicated phosphorylated integrin β 1 following the orientation of fibers. (c-i) Representative Western blots and semiquantification of integrin proteins. (c-ii) Representative Western blots and semiquantification of FAK and p-FAK signaling pathways before and after treatment with the G0187 inhibitor and ERK1/2 and p-ERK1/2 signaling before and after treatment with the U0126 inhibitor. *p < 0.05, **p < 0.01, ***p < 0.001, ns: nonsignificant.

ECM proteins including collagen and noncollagenous proteins (NCPs) started to deposit within the constructs, but not high enough by 7 days to drastically change the overall mechanical performance. However, there is some noticeable change to LA-AF-45 with increased strain, suggesting more deposition of collagen and NCPs. By day 21 of culture, the mineralization became dominant (see Figures 5a and S8, Supporting Information). Elevated mineralization of cultured constructs would expectedly increase the mechanical strength and decrease the elongation capacity. Indeed, tensile testing of various constructs showed that the 21-day LA-AF-45

constructs had a breaking strength of 170.5 kPa, which was significantly higher than that of the 21-day LA-RF constructs (90.9 kPa) (Figure 5d), while the elongation at break also significantly reduced from 77% (LA-RF) down to 26% (LA-AF-45). As expected, the highest breaking strength was obtained with 21-day LA-AF-0 constructs (530 kPa) with the breaking strain of only 15%. We believe that such drastic changes in mechanical properties of the cultured multilayered assembly of cell-laden fibrous matrices are mainly attributed to the time-dependent accumulation of minerals, and this is especially true with those 21-day constructs as significant

mineralization normally takes place around 21 days in vitro. 15 In fact, this phenomenon is similarly seen with the natural bone matrix found in the regions requiring flexible tension and tough bone,²⁹ in which the angularly oriented lamellae of mineralized collagen fibers tend to have greater strain and ductile properties than singular arrays of the stacked mineralized collagen fibers, which can be distinguished under the polarized light with a distinct bright and dark bone, resulting from the unique organization of mineralized collagen fibers within the bone matrix.²⁷ Notably, during the early culture prior to pronounced ECM synthesis, the anisotropic fiber organization would dominate the mechanical performance of assembled constructs; however, with prolonged culture, the AF-induced collagen synthesis and subsequent uniform hydroxyapatite deposition between/within the newly formed collagen fibrils by hBMSCs would become predominant to increase the stress and brittleness of 3D LA-AF-0/45, thereby leading to a reduction in its elongation at break. Clearly, the L-b-L assembly of cell-laden AF matrices allows to partially replicate the representative attributes of the natural mineralized bone matrix in terms of mechanical properties.

3.5. Involvement of Integrins in the Overlay Angle-Induced Osteogenic Differentiation of hBMSCs. As the essential mediators for outside-in signaling, integrins play an important role in sensing those physical and topological cues of their residing environment and transmitting such stimuli intracellularly for downstream regulations, 30° which would also be applicable to the overlay angle-induced osteogenic differentiation of hBMSCs. Thus, time-resolved analysis of the gene expression of selected integrins (e.g., $\alpha 2$, $\beta 1$), involved in collagen fiber-associated cell binding, would help to unfold the possible mechanistic regulation of BMSC osteogenic differentiation by the overlay angle of the AF assembly. As shown in the real-time PCR analysis on relative genes (Figure 6a), the cells within the LA-AF-0/45 assembly showed an elevated expression of integrin subunits $\alpha 2$, $\alpha 3$, and $\beta 1$ as early as 7 days compared with those in the LA-RF assembly. Compared to integrins $\alpha 2$ and $\alpha 3$, a more pronounced upregulation of the integrin β 1 subunit was seen by 14 days with both the LA-AF-45/0 assembly despite a slightly higher level with LA-AF-0 ones (Figure 6a). Such an elevation most likely comes from the AF-induced increase of promoter genes, which subsequently induce the transcription of integrin genes for mRNA. With that said, the outside-in signaling turns into the inside-out ones³¹ to further regulate the osteogenic differentiation process of BMSCs. Further comparison of gene expression between LA-AF-0 and LA-AF-45 revealed a consistent increase of the integrin α 2 subunit in the LA-AF-0 assembly for all of the investigating time points and a noticeable increase of integrin β 1 in the LA-AF-0 assembly for days 14 and 21 (Figure 6a). Taken together, it is reasonable to conclude that the LA-AF-0 assembly promotes the expression of integrin $\alpha 2\beta 1$. Western blotting results also confirmed a similar trend in the protein expression of integrin $\alpha 2$ and $\alpha 3$ among different assembled constructs, and a significantly higher-level integrin β 1 protein, about 2-fold, was seen only with the LA-AF-0 assembly but not LA-AF-45 ones in comparison to the LA-RF assembly (Figure 6c-i). Actually, LA-AF-45 and LA-RF assemblies displayed a comparable integrin β 1 level. And such an observation is somewhat interesting, implying that the overlay angle of 45° of AF might induce a cellular response to hBMSCs similar to that by RF upon prolonged culture. The use of HUST-4 to detect activated integrin β 1, i.e., phosphorylated integrin β 1 via

immunoprecipitation, has shown an elevated level of active integrin β 1 in both LA-AF-0/45 in comparison to LA-RF, but is much more pronounced in LA-AF-0 (Figure 6c-i). Comparing the expression of total integrin $\beta 1$, AF alone could promote integrin $\beta 1$ activation, which is consistent with our previous observation, 32 but could lead to further enhancement of such an activation within the 3D parallelassembled AF constructs (i.e., LA-AF-0). Immunofluorescence staining of active integrin β 1 by HUST-4 further illustrated the regulatory role of the fiber orientation. Notably, a strong fluorescence of HUST-4 (yellow arrows), closely following AF, was seen in LA-AF-0/45 (Figure 6b), but not in LA-RF (the green fluorescence is a nonspecific artifact). The slight distribution difference in HUST-4 fluorescence was also noticed between LA-AF-0 and LA-AF-45, i.e., single-directional orientation in LA-AF-0 versus two-directional orientations, which is attributed to the different overlay angles of the AF

To interrogate the involvement of integrins in the osteogenic differentiation of hBMSCs regulated by the overlay angle of the AF assembly, its downstream signaling was further studied. Focal adhesion kinase (FAK)-extracellular signal-regulated kinase (ERK) 1/2 is an important pathway involved in the osteogenic differentiation and mineralization of hBMSCs.³³ It was shown that $\alpha 3\beta 1/\alpha 2\beta 1$ integrins could upregulate the osteogenic transcription factor RUNX2 and NCPs (OPN, OCN)31 and induced RUNX2/CBFA-1 phosphorylation for subsequent expression of OPN, OCN, and ALP through FAK/ ERK.³⁴ FAK, a cytoplasmic tyrosine kinase, is triggered upon the binding of integrin to the ECM. ²⁹ Its downstream ERK is a member of the mitogen-activated protein kinase (MAPK) family.³⁵ Western blot analysis was performed to analyze total FAK and its phosphorylation at Tyr-397 (p-FAK). As expected, hBMSCs from either the LA-AF-0 or LA-AF-45 assembly had the increase of total FAK and p-FAK (Figure 6cii) and the culture treated with the integrin $\alpha 2\beta 1$ inhibitor, G0187, significantly reduced the level of total FAK and almost abolished the phosphorylation of FAK, confirming the participation of integrin $\alpha 2\beta 1$ in the downstream regulation of FAK. As an important pathway to promote osteogenic differentiation and bone formation in vitro and in vivo, 15 we further studied the ERK MAPK pathway by examining the expression level of ERK1/2 and its phosphorylation, which is the downstream mediator of FAK. Interestingly, the total ERK1/2 level for all of the L-b-L assembled constructs was comparable if not identical; however, a noted difference was observed in the level of phosphorylated ERK1/2 (p-ERK1/2), in which both LA-AF-0/45 exhibited a noticeable elevation compared to LA-RF but a much higher increase with LA-AF-0 (Figure 6c-ii). We also investigated the expression of two representative osteogenic markers (RUNX2 and OCN) to affirm the involvement of ERK1/2 in AF and the overlay angleinduced osteogenic differentiation of BMSCs. To ensure the regulation of osteogenic markers by ERK1/2 phosphorylation, a phosphorylation inhibitor U0126 was used to block the ERK1/2 phosphorylation, which did significantly reduce the p-ERK1/2 level, as confirmed by Western blotting (Figure 6c-ii). Subsequently, the characteristic osteogenic protein (RUNX2, OCN) of LA-AF was decreased compared with that before inhibition. To our surprise, inhibition of p-ERK1/2 led to much more attenuation of RUNX2 in LA-AF-0 than in LA-AF-45, implying the pivotal role of p-ERK1/2 in regulating the osteogenic differentiation of hBMSCs within LA-AF-0, but not

much in LA-AF-45 (Figure 6c-ii). The decrease in OCN was also observed with the ERK1/2 inhibition, but less pronounced compared to RUNX2. Early study suggests the involvement of OCN in regulating the bone mechanical strength possibly through the increase in bone mass;³⁶ however, the recent findings also indicate that OCN enhances bone strength by aligning the orientation of the Hap crystal c-axis parallel to collagen fibers instead.³⁷ All of the above results indicated that the 0° overlay angle of the cell-laden AF assembly enhanced ERK1/2 phosphorylation, which was also seen with the 45° overlay angle, but lower than the former. Altogether, RUNX2, the highly oriented organization of cell-laden AF matrices in LA-AF-0 constructs triggered the upregulation of integrin $\alpha 2\beta 1$, which subsequently activated the FAK/ERK1/2 pathways to promote the osteogenic differentiation of hBMSCs for collagen synthesis and mineralization (Figures 4 and 5).

4. CONCLUSIONS

In this study, we effectively demonstrated the possibility of replicating the lamellae-like organization by the L-b-L assembly of cell-laden AF matrices of core (PCL/Col I)-shell (Col I) nanofibers. During the assembly, the flexibility to rotate the overlay angle for each cell-laden AF layer not only conformationally matches the rotational stacking pattern of mineralized collagen lamellae of the natural bone but also architecturally and compositionally emulates the bone matrix at the nanoscale. With such unique constructs, we examined the effect of the overlay angle for the AF assembly on the osteogenic differentiation of hBMSCs and the regulatory mechanism behind. In summary, the ECM fibers of the bone matrix can convey the topological stimuli to the residing cells via cell membranous integrin $\alpha 2\beta 1$, which subsequently modulates its downstream pathways (FAK, MAPK/ERK1/2), and ultimately relays the outside signals to alter the genetic phenotypes for further inside-out signaling. Clearly, the findings from the current study also provide the guidance to design and fabricate bonelike structures with a compositional and spatial complexity similar to the natural bone.

ASSOCIATED CONTENT

Supporting Information

The Supporting Information is available free of charge at https://pubs.acs.org/doi/10.1021/acsami.4c12847.

Primers for the genes related to osteogenic differentiation of hBMSCs (Table S1); layer-by-layer assembly of cell-laden nanofiber membranes into 3D constructs (Figure S1); SEM micrographs of the electrospun core-shell nanofibers with distinct fiber organizations (Figure S2); time-resolved degradation of electrospun core-shell nanofibers (Figure S3); representative images of subcutaneously implanted nanofibrous matrices (Figure S4); SEM micrograph and reconstructed confocal image of the stacked nanofiber membranes (Figure S5); time-dependent expression of the ALP gene in hBMSCs (Figure S6); the level of selected osteogenic marker proteins expressed by hBMSCs (Figure S7); representative microscopic images of LA-RF and LA-AF-45/0 (Figure S8) (PDF)

Confocal video of LA-AF-45 and LA-AF-0 (Video S1a) (MP4)

Video S1b (MP4)

Video S2a (MP4)

Video S2b (MP4)

AUTHOR INFORMATION

Corresponding Authors

Hong Li – College of Chemistry and Materials Science, Jinan University, Guangzhou 510632 Guangdong, China; orcid.org/0000-0003-2315-5235; Email: tlihong@ jnu.edu.cn

Hongjun Wang – Department of Biomedical Engineering, Stevens Institute of Technology, Hoboken, New Jersey 07030, United States; Semcer Center for Healthcare Innovation and Department of Chemistry and Chemical Biology, Stevens Institute of Technology, Hoboken, New Jersey 07030, United States; orcid.org/0000-0003-3455-8523; Email: Hongjun.Wang@stevens.edu

Authors

Shuyun Zhang - Guangdong Police College, Guangzhou 510440 Guangdong, China; College of Chemistry and Materials Science, Jinan University, Guangzhou 510632 Guangdong, China; Semcer Center for Healthcare Innovation, Stevens Institute of Technology, Hoboken, New *Jersey 07030, United States;* orcid.org/0000-0002-3453-

Dengjian Qu - College of Chemistry and Materials Science, Jinan University, Guangzhou 510632 Guangdong, China Bowen Luo - Department of Biomedical Engineering, Stevens Institute of Technology, Hoboken, New Jersey 07030, United States; Semcer Center for Healthcare Innovation, Stevens Institute of Technology, Hoboken, New Jersey 07030, United States; orcid.org/0009-0005-1293-8690

Lichen Wang - Department of Biomedical Engineering, Stevens Institute of Technology, Hoboken, New Jersey 07030, United States; Semcer Center for Healthcare Innovation, Stevens Institute of Technology, Hoboken, New Jersey 07030, **United States**

Complete contact information is available at: https://pubs.acs.org/10.1021/acsami.4c12847

Author Contributions

*S.Z. and D.Q. authors contributed equally to this work.

The authors declare no competing financial interest.

ACKNOWLEDGMENTS

This study was financially supported by the National Science Foundation (NSF-GCR award number 2219014), the NIAMS award number 1R01AR067859, the Established Investigator Grant award from MTF Biologics, the National Natural Science Foundation of China (NSFC-32301134, Youth Science Foundation Project), the National Natural Science Foundation of China (31971284), and the GuangDong Basic and Applied Basic Research Foundation (2024A1515013268).

REFERENCES

(1) Sivakumar, P. M.; Yetisgin, A. A.; Sahin, S. B.; Demir, E.; Cetinel, S. Bone tissue engineering: Anionic polysaccharides as promising scaffolds. Carbohydr. Polym. 2022, 283, No. 119142.

(2) Shi, H.; Zhou, K.; Wang, M.; Wang, N.; Song, Y.; Xiong, W.; Guo, S.; Yi, Z.; Wang, Q.; Yang, S. Integrating physicomechanical and biological strategies for BTE: biomaterials-induced osteogenic differentiation of MSCs. Theranostics 2023, 13 (10), 3245.

- (3) Gao, X.; Yang, J.; Gan, X.; Lin, Y.; Xu, J.; Shan, Z.; Han, Z.; Chen, S.; Huang, B.; Fan, B.; Chen, Z. Optimized DLP 3D-printed high-resolution nano zirconia-hydroxyapatite scaffold with craniomaxillofacial soft tissue invasion resistance and pro-osteogenic properties via dectin-1/syk inflammatory axis. *Chem. Eng. J.* **2024**, 491, No. 152044.
- (4) Safari, B.; Davaran, S.; Aghanejad, A. Osteogenic potential of the growth factors and bioactive molecules in bone regeneration. *Int. J. Biol. Macromol.* **2021**, *175*, 544–557.
- (5) Huo, S.-C.; Yue, B. Approaches to promoting bone marrow mesenchymal stem cell osteogenesis on orthopedic implant surface. *World J. Stem Cells* **2020**, *12* (7), 545.
- (6) Collins, M. N.; Ren, G.; Young, K.; Pina, S.; Reis, R. L.; Oliveira, J. M. Scaffold fabrication technologies and structure/function properties in bone tissue engineering. *Adv. Funct. Mater.* **2021**, *31* (21), No. 2010609.
- (7) Wang, J.; Yang, Q.; Saiding, Q.; Chen, L.; Liu, M.; Wang, Z.; Xiang, L.; Deng, L.; Chen, Y.; Cui, W. Geometric angles and gene expression in cells for structural bone regeneration. *Adv. Sci.* **2023**, *10* (32), No. 2304111.
- (8) Liu, Y.; Li, A.; Li, Y.; Chen, S. Bionic design based on micronano structure of osteon and its low-velocity impact damage behavior. *Bioresources Bioprocess.* **2022**, 9 (1), 115.
- (9) Vom Scheidt, A.; Hemmatian, H.; Püschel, K.; Krause, M.; Amling, M.; Busse, B. Bisphosphonate treatment changes regional distribution of trabecular microstructure in human lumbar vertebrae. *Bone* **2019**, *127*, 482–487.
- (10) Guo, Z.; Xu, J.; Ding, S.; Li, H.; Zhou, C.; Li, L. In vitro evaluation of random and aligned polycaprolactone/gelatin fibers via electrospinning for bone tissue engineering. *J. Biomater. Sci., Polym. Ed.* **2015**, 26 (15), 989–1001.
- (11) He, P.; Li, Y.; Huang, Z.; Guo, Z.-Z.; Luo, B.; Zhou, C.-R.; Li, H. A multifunctional coaxial fiber membrane loaded with dual drugs for guided tissue regeneration. *J. Biomater. Appl.* **2020**, *34* (8), 1041–1051.
- (12) Chen, X.; Fu, X.; Shi, J.-g.; Wang, H. Regulation of the osteogenesis of pre-osteoblasts by spatial arrangement of electrospun nanofibers in two-and three-dimensional environments. *Nanomed.: Nanotechnol., Biol. Med.* **2013**, 9 (8), 1283–1292.
- (13) Lu, P.; Liu, R.; Lu, D.; Xu, Y.; Yang, X.; Jiang, Z.; Yang, C.; Yu, L.; Lei, X.; Chen, Y. Chemical screening identifies ROCK1 as a regulator of migrasome formation. *Cell Discovery* **2020**, *6* (1), 51.
- (14) Wang, Y.; Morsali, R.; Dai, Z.; Minary-Jolandan, M.; Qian, D. Computational nanomechanics of noncollagenous interfibrillar interface in bone. ACS Appl. Mater. Interfaces 2020, 12 (22), 25363–25373.
- (15) Zhang, S.; Luo, X.; Guo, C.; Huang, K.; Ding, S.; Li, L.; Zhou, C.; Li, H. Tissue engineered bone via templated hBMSCs mineralization and its application for bone repairing. *Biomater. Adv.* **2022**, *139*, No. 212937.
- (16) Shao, Z.; Zhang, X.; Song, Z.; Liu, J.; Liu, X.; Zhang, C. Simulation Guided Coaxial Electrospinning of Polyvinylidene Fluoride Hollow Fibers with Tailored Piezoelectric Performance. *Small* **2023**, *19*, No. 2303285.
- (17) Luo, X.; Zhang, S.; Luo, B.; Li, H. Engineering collagen fiber templates with oriented nanoarchitecture and concerns on osteoblast behaviors. *Int. J. Biol. Macromol.* **2021**, *185*, 77–86.
- (18) Karmakar, R.; Dey, S.; Alam, A.; Khandelwal, M.; Pati, F.; Rengan, A. K. Attributes of Nanomaterials and Nanotopographies for Improved Bone Tissue Engineering and Regeneration. *ACS Appl. Bio Mater.* **2023**, *6* (10), 4020–4041.
- (19) Singh, S. J.; Turner, W.; Glaser, D. E.; McCloskey, K. E.; Filipp, F. V. Metabolic shift in density-dependent stem cell differentiation. *Cell Commun. Signaling* **2017**, *15*, 44.
- (20) Bispo, D. S. C.; Jesus, C. S.; Correia, M.; Ferreira, F.; Bonifazio, G.; Goodfellow, B. J.; Oliveira, M. B.; Mano, J. F.; Gil, A. M. NMR metabolomics assessment of osteogenic differentiation of adiposetissue-derived mesenchymal stem cells. *J. Proteome Res.* **2022**, *21* (3), 654–670.

- (21) Kong, B.; Sun, L.; Liu, R.; Chen, Y.; Shang, Y.; Tan, H.; Zhao, Y.; Sun, L. Recombinant human collagen hydrogels with hierarchically ordered microstructures for corneal stroma regeneration. *Chem. Eng. J.* **2022**, 428, No. 131012.
- (22) Alford, A. I.; Kozloff, K. M.; Hankenson, K. D. Extracellular matrix networks in bone remodeling. *Int. J. Biochem. Cell Biol.* **2015**, 65, 20–31.
- (23) Shrestha, S.; Tieu, T.; Wojnilowicz, M.; Voelcker, N. H.; Forsythe, J. S.; Frith, J. E. Delivery of miRNAs Using Porous Silicon Nanoparticles Incorporated into 3D Hydrogels Enhances MSC Osteogenesis by Modulation of Fatty Acid Signaling and Silicon Degradation. *Adv. Healthcare Mater.* **2024**, *13*, No. 2400171.
- (24) Bailey, S.; Karsenty, G.; Gundberg, C.; Vashishth, D. Osteocalcin and osteopontin influence bone morphology and mechanical properties. *Ann. N. Y. Acad. Sci.* **2017**, 1409 (1), 79–84.
- (25) Liu, X.; Ren, Z.; Meng, X.; Xu, Y. Substrate topography regulates extracellular matrix component secretion by bone marrow-derived mesenchymal stem cells. *J. Sci.: Adv. Mater. Dev.* **2022**, 7 (2), No. 100437.
- (26) Ma, C.; Du, T.; Niu, X.; Fan, Y. Biomechanics and mechanobiology of the bone matrix. *Bone Res.* **2022**, *10* (1), 59.
- (27) Stockhausen, K. E.; Qwamizadeh, M.; Wölfel, E. M.; Hemmatian, H.; Fiedler, I. A.; Flenner, S.; Longo, E.; Amling, M.; Greving, I.; Ritchie, R. O.; et al. Collagen fiber orientation is coupled with specific nano-compositional patterns in dark and bright osteons modulating their biomechanical properties. *ACS Nano* **2021**, *15* (1), 455–467.
- (28) Kubi, J. A.; Brah, A. S.; Cheung, K. M. C.; Lee, Y. L.; Lee, K.-F.; Sze, S. C. W.; Qiao, W.; Yeung, K. W.-K. A new osteogenic protein isolated from Dioscorea opposita Thunb accelerates bone defect healing through the mTOR signaling axis. *Bioact. Mater.* **2023**, 27, 429–446.
- (29) Gauthier, R.; Follet, H.; Langer, M.; Peyrin, F.; Mitton, D. What is the influence of two strain rates on the relationship between human cortical bone toughness and micro-structure? *Proc. Inst. Mech. Eng., Part H* **2020**, 234 (3), 247–254.
- (30) Yin, B.; Zhang, Q.; Yan, J.; Huang, Y.; Li, C.; Chen, J.; Wen, C.; Wong, S. H. D.; Yang, M. Nanomanipulation of Ligand Nanogeometry Modulates Integrin/Clathrin-Mediated Adhesion and Endocytosis of Stem Cells. *Nano Lett.* **2023**, 23 (19), 9160–9169.
- (31) Leem, Y. H.; Lee, K. S.; Kim, J. H.; Seok, H. K.; Chang, J. S.; Lee, D. H. Magnesium ions facilitate integrin alpha 2-and alpha 3-mediated proliferation and enhance alkaline phosphatase expression and activity in hBMSCs. *J. Tissue Eng. Regener. Med.* **2016**, *10* (10), E527–E536.
- (32) Huang, C.; Fu, X.; Liu, J.; Qi, Y.; Li, S.; Wang, H. The involvement of integrin $\beta 1$ signaling in the migration and myofibroblastic differentiation of skin fibroblasts on anisotropic collagen-containing nanofibers. *Biomaterials* **2012**, 33 (6), 1791–1800.
- (33) Prasadam, I.; van Gennip, S.; Friis, T.; Shi, W.; Crawford, R.; Xiao, Y. ERK-1/2 and p38 in the regulation of hypertrophic changes of normal articular cartilage chondrocytes induced by osteoarthritic subchondral osteoblasts. *Arthritis Rheumatol.* **2010**, *62* (5), 1349–1360
- (34) Chen, C.; Jiang, Z.; Yang, G. Laminins in osteogenic differentiation and pluripotency maintenance. *Differentiation* **2020**, *114*, 13–19.
- (35) Li, S.; Wu, H.; Wang, F.; Kong, L.; Yu, Y.; Zuo, R.; Zhao, H.; Xu, J.; Kang, Q. Enhanced Bone Regeneration through Regulation of Mechanoresponsive FAK-ERK1/2 Signaling by ZINC40099027 during Distraction Osteogenesis. *Int. J. Med. Sci.* **2024**, 21 (1), 137.
- (36) Xu, L.; Fang, J.; Pan, J.; Qi, H.; Yin, Y.; He, Y.; Gan, X.; Li, Y.; Li, Y.; Guo, J. Zinc finger-inspired peptide-metal-phenolic nanointerface enhances bone-implant integration under bacterial infection microenvironment through immune modulation and osteogenesis promotion. *Bioact. Mater.* **2024**, *41*, 564–576.
- (37) Komori, T. What is the function of osteocalcin? *J. Oral Biosci.* **2020**, 62 (3), 223–227.